

Approximate universality in the electric field variation on a field-emitter tip in the presence of space charge

Raghwendra Kumar,¹ Gaurav Singh,^{1,2} and Debabrata Biswas^{1,2, a)}

¹⁾*Bhabha Atomic Research Centre, Mumbai 400 085, INDIA*

²⁾*Homi Bhabha National Institute, Mumbai 400 094, INDIA*

The electric field at the surface of a curved emitter is necessary to calculate the field emission current. For smooth parabolic emitting tips where space charge is negligible, variation of the electric field at the surface is known to follow the generalized cosine law. Here we investigate the validity of the cosine law in the regime where space charge due to emitted electrons is important. Particle-in-Cell (PIC) simulations with an emission algorithm based on the cosine law is employed for this study. It is shown that if E_P and E_L be the field at the apex of tip with and without space charge respectively, then for $\vartheta = E_P/E_L \geq 0.9$, the average relative deviation of the electric field from the cosine law is less than 3% over the endcap. Thus, an emission scheme based on cosine law may be used in PIC simulations of field emission of electrons from curved emitter tips in the weak space charge regime. The relation between ϑ and normalized current ζ for curved emitters in this regime is also investigated. A linear relation, $\vartheta = 1 - \delta\zeta$ (where δ is a constant), similar to that obtained theoretically for flat emitting surfaces is observed but the value of δ indicates that the extension of the theory for curved emitters may require incorporation of the field enhancement factor.

I. INTRODUCTION

Field emission is one of the important mechanisms of electron emission from the surface of a material. The theory of field emission was first formulated by Fowler and Nordheim (FN) in the year 1928^{1,2}. Since then several important aspects of field emission theory have been studied by researchers³⁻¹⁵ and it is now increasingly being accepted that the curvature-corrected Murphy-Good formalism currently offers the best description of field emission^{16,17}.

The expression for the emitted current density at a point on the surface of emitter based on Murphy-Good⁴ formulation reads as:

$$J(\mathbf{r}) = \frac{1}{t_F^2} \frac{A_{FN}}{\phi} (E_L(\mathbf{r}))^2 \exp\left(-B_{FN} v_F \phi^{3/2} / E_L(\mathbf{r})\right). \quad (1)$$

Here $A_{FN} \simeq 1.541434 \mu\text{A eV V}^{-2}$, $B_{FN} \simeq 6.830890 \text{ eV}^{-3/2} \text{ V nm}^{-1}$ are the conventional Fowler-Nordheim constants while $v_F = 1 - f + (f/6) \ln f$ and $t_F = 1 + f/9 - (f/18) \ln f$ are corrections due to the image charge potential with $f \simeq c_S^2 E_L(\mathbf{r})/\phi^2$ where c_S is the Schottky constant and $c_S^2 = 1.439965 \text{ eV}^2 \text{ V}^{-1} \text{ nm}$. $E_L(\mathbf{r})$ refers to the local electric field on the emitter surface, while ϕ is the work function of the emitter material which we shall consider to be 4.5eV. Eq. (1) is best suited^{13,15} when the apex radius of curvature $R_a > 100\text{nm}$ and we shall stick to this regime through the rest of the paper.

It is well known that field emission of electrons from a surface requires a high electric field, typically $> 3 \text{ V/nm}$ for an emitter having work function $\phi = 4.5\text{eV}$. The local field enhancement at a curved surface due to geometrical

effects makes it possible to generate such high local fields even at relatively lower applied macroscopic electric field. The local field enhancement factor γ is the ratio of local electric field to the asymptotic electric field E_0 , away from emitting surface¹⁸⁻²¹. It may be noted that the maximum field enhancement occurs at the apex of the curved emitting structure²⁰.

To get the total current emitted from the tip, knowledge of the electric field at all the points on emitting surface is important. For axially symmetric emitters with locally parabolic tips, it has been shown that the magnitude of the local electric field E_l at the surface of the emitter $z = z(\rho)$ follows a ‘universal’ cosine law^{22,23}

$$E_l(\tilde{\theta}) = E_a \cos \tilde{\theta} \quad (2)$$

$$\cos \tilde{\theta} = \frac{z/h}{\sqrt{(z/h)^2 + (\rho/R_a)^2}}. \quad (3)$$

In the above, E_a denotes the electric field at the apex, h is height of the emitter, R_a is radius of curvature at apex of the emitter and ρ is the distance of point on the surface from the axis of emitter. Thus, the net current obtained by integrating Eq. (1) over the emitter surface $z = z(\rho)$, can be expressed in terms of the apex electric field E_a and the apex radius of curvature R_a since the electric field at any point on the surface is related to apex electric field using Eqns. (2) and (3). Thus, if the cosine law is valid, it is necessary to determine only the apex electric field accurately in order to predict the net field emission current.

Note that the locally parabolic assumption $z \approx h - \rho^2/(2R_a)$ includes all generic emitters with a smooth endcap, although the extent upto which parabolicity holds depends on the nature of the endcap. Thus, for a hemispherical endcap for instance, the parabolic approximation holds close to the apex and can therefore be used only for low electric fields. A hemiellipsoid endcap on

^{a)}Electronic mail: dbiswas@barc.gov.in

the other hand, with height greater than $3R_a$ follows the parabolic approximation further away from the apex and can be used to predict the net current at higher local field strengths.

The cosine law greatly simplifies the job of calculating the net emitted current. It can also be profitably used for emission-modeling in Particle-In-Cell²⁴ (PIC) simulation²⁵. The standard approach in PIC codes is to solve Maxwell's equations, obtain the field on the emitting surface and then use Eq. (1) to get the emission current from each surface area element. The charge per time-step can then be evaluated and computational particles launched from each area element normal to the surface. In case of a curved emitter tip however, the accurate evaluation of charge emitted at each time step from sufficiently fine surface elements on the emitting object, adds to the computational resources enormously in a Finite Difference Time Domain (FDTD) based PIC simulation. An alternate emission method in a PIC code²⁵, is to use the generalized cosine law^{22,23} to arrive at the net emission current using only the apex electric field and the apex radius of curvature. A knowledge of the electric field variation on the emitter endcap (the generalized cosine law) also enables us to cast the distribution of electrons emitted in a geometry-independent universal form, in terms of the generalized angle $\tilde{\theta}$, the total energy and the normal energy²⁶. Thus, while the alternate approach still requires a solution to the Poisson equation, only the apex field needs to be sufficiently accurate to capture the total emission current. The charge per time step can then be divided into a desired number of computational particles and the particles can be emitted using distributions for the angle $\tilde{\theta}$ and conditional distributions for the normal energy \mathcal{E}_N and total energy \mathcal{E}_T .

The cosine law can thus reduce the computational burden in PIC simulations. It has been shown to hold for different kind of emitter geometries²³. Although, it was originally derived for the anode far away from the emitter apex, it holds for the anode in close proximity to the emitter²⁷ as well as in the presence of other emitters such as in an array or a random arrangement of emitters²⁸. In fact, numerical simulations show that it is also valid for gated emitters¹⁷ and multiscale geometries^{25,29}.

To the best of our knowledge, it is not known whether the cosine law holds in the presence of space charge in the diode region. This is crucial for the determination of the net emitted current using the apex electric field and the subsequent use of the distribution based particle-injection discussed above. We have attempted to address this question in this communication. Due to the high sensitivity of field emission current on the local electric field at the emitting surface, a small change in electric field can result in a large change in the emitted current. The presence of charges in the diode reduces the field on the emitter surface resulting in a reduction in emitted current³⁰⁻³⁵. This type of limitation in current due to space charge is different from space charge limited emission in case of thermal or explosive field emitters. This

phenomenon, where relatively weak space charge limits the current by affecting field emission from the emitting surface, has been referred to as field-emitted vacuum space charge (FEVSC) by Forbes³² or space charge affected field emission (SCAFE) by Jensen et. al³⁴. We shall investigate the validity of cosine law in this regime.

The paper is organized as follows. We first describe the method employed to test the validity of cosine law in section II. The geometry of the diode and other details about simulation are given in section III. This is followed by numerical results and analysis in section IV. Concluding remarks will be presented in section V.

II. METHODOLOGY

The question of validity of the cosine law in the presence of space charge is investigated in this communication using the Particle-in-Cell (PIC) simulation technique. PIC simulation involves (i) update of electric and/or magnetic field on computational grid by solving Maxwell equations (ii) movement of charged particles under the influence self generated and/or imposed electric and magnetic field and (iii) assignment of charge and current density due to charged particles at the computational grid to update the field. In general, PIC codes employ finite difference method. This may be attributed to robustness of algorithms for assignment of charge and current density in finite difference approach.

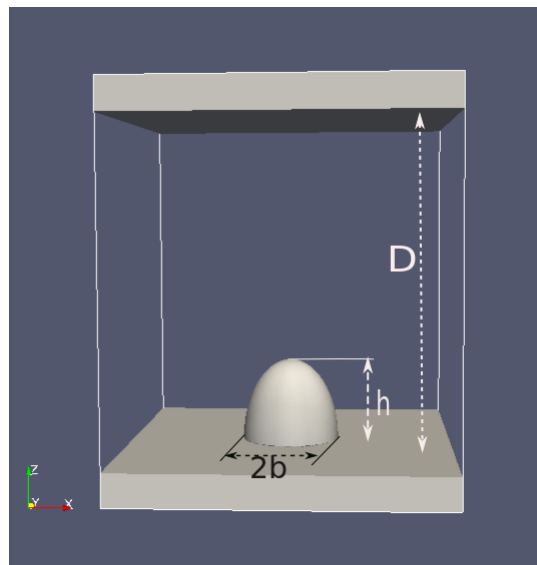


FIG. 1. Geometry of the diode modeled in PASUPAT. D is diode gap, h and b are the height and base radius of the hemi-ellipsoidal emitter respectively.

A regular computational grid poses challenge in handling surfaces of curved boundaries. As the computational cells at the curved boundaries are cut into two

medium by a boundary surface, special algorithms are required to smoothen the field³⁶. Emission of charged particle using Eq. 1 from such cells also requires special care^{37,38}.

Furthermore, in order to model the electron flow in a diode properly, the computational time step should be small compared to the transit time of the particle. Note that the ballistic transit time is given by $T_{transit} = \sqrt{2mD/eE_0}$, where D is the diode gap-length. For a micrometer size emitting tip, an accurate estimation of the field requires the grid to be sufficiently fine. Thus, the area of the element at the emitting surface in a cut-cell is very small. As a result, the amount of charge emitted from such an element in a computational time step turns out to be less than the charge of an electron. This poses a problem as far as convergence with respect to the number of computational particles is concerned since the charge per particle moves further away from the charge of the physical particles being modeled.

Recently, an emission algorithm based on cosine law of field variation at emitting tip was used in a study of electron beam transport across a gated diode²⁵. The space charge effect on the emission was negligible in that study and hence the cosine law was assumed to be valid. The emission algorithm involves: (i) estimation of charge emitted from the emitting tip¹¹ using a combination of Eq. 1 and the cosine law (ii) divide the charge into a number of computational macro-particles (iii) emit the particles from area lying between $\tilde{\theta}$ to $\tilde{\theta} + \Delta\tilde{\theta}$ by sampling $\tilde{\theta}$ using distribution function derived in Ref. [11]. The distribution function reads:

$$f(\tilde{\theta}) = 2\pi R_a^2 \frac{\sin \tilde{\theta}}{\cos^2 \tilde{\theta}} J(\tilde{\theta}) \frac{\tilde{z}^3}{C_1} C_0 \quad (4)$$

where the quantities \tilde{z} , C_0 and C_1 are defined in the appendix . For sharp emitters ($h/R_a \gg 1$), further simplification can be made and the distribution function assumes the form:

$$f(\tilde{\theta}) \simeq 2\pi R_a^2 \frac{\sin \tilde{\theta}}{\cos^2 \tilde{\theta}} J(\tilde{\theta}). \quad (5)$$

As mentioned in Ref. [25], first $\tilde{\theta}$ is sampled from the distribution described above. The value of the normal energy \mathcal{E}_N and total energy \mathcal{E}_T are thereafter obtained using the conditional distributions $f(\mathcal{E}_N|\tilde{\theta})$ and $f(\mathcal{E}_T|\mathcal{E}_N, \tilde{\theta})$ respectively. These distributions can be arrived at using the joint distribution $f(\tilde{\theta}, \mathcal{E}_N, \mathcal{E}_T)$ ¹¹. Once the angle $\tilde{\theta}$, normal energy and total energy are calculated, velocity components in local co-ordinate system are obtained using suitable transformations.

Our rationale in investigating the validity of cosine law in the presence of space charge is as follows. As there is no charge in the diode gap at the start of the simulation, the cosine law is valid and hence charged particles (computational particle in PIC) are emitted using the distribution

TABLE I. Geometric parameters considered in the study

Geometry	$D(\mu\text{m})$	$h(\mu\text{m})$	$b(\mu\text{m})$
1	1.0	0.2515	0.15
2	10.0	2.515	1.5
3	100.0	25.15	15

function described above. As space charge builds up in the diode region, the apex electric field changes. The field solver of the PIC code calculates the net field at the apex of the emitting tip, and this field in turn is used for further emission using the distribution function. The electric field at the surface of emitter is recorded at different times and its variation along the surface is studied to see whether it follows the cosine law. If the deviation from the cosine law is large, it can be concluded that the emission algorithm is invalid. On the other hand, if the deviation is small even after achieving the steady state, the cosine law holds and the emission algorithm is valid for the parameters of the diode.

III. GEOMETRY AND SIMULATION DETAILS

We have carried out simulation study using the PIC code PASUPAT^{25,39}. A parallel plate diode with hemi-ellipsoidal emitter on the cathode plate has been considered in the simulation as shown in Fig 1. Different values of diode gap-length D , emitter height h and base radius b have been considered (see table I). The hemi-ellipsoidal emitter is placed at the center of the cathode plate. The orientation of the emitter is along the z direction. The anode plate is kept at $z = D$ from the cathode plate. Periodic boundary conditions are imposed along x and y boundaries which are kept sufficiently away from the hemi-ellipsoidal emitter to simulate an isolated emitter.

The number of computational cells along x , y and z were typically taken to be $n_x = 128$, $n_y = 128$ and $n_z = 256$. We have varied the grid, time-step and particle number to ensure convergence. The Cut-Cell module³⁶ of PASUPAT has been deployed to model curved emitter. Since an electrostatic simulation has been carried out, a Multigrid Poisson solver⁴⁰ has been used to update the electric field. The emission module described in Sec. II is used to estimate the net field emission current, the number of computational particles to be emitted in a time step, the distribution on the endcap with respect to the angle $\tilde{\theta}$ and finally the initial velocities of the particles.

IV. RESULTS

In this study three geometries have been considered. Parameters (D, h, b) of the respective geometries 1,2, and 3 are specified in Table I.

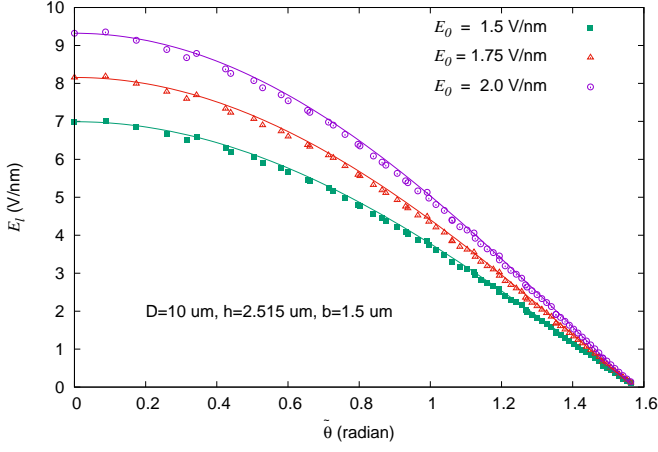


FIG. 2. Variation of electric field on the surface with generalized angle $\tilde{\theta}$ for three different values of asymptotic electric field E_0 at the start of simulation ($t = 0$) for Geometry 2. Points are values obtained using PASUPAT PIC simulation while the solid curves correspond to $E_a \cos \tilde{\theta}$. Clearly, the electric field follows the cosine law in the absence of space charge.

We shall first consider Geometry 2 and compare the magnitude of electric field on the surface of the emitter at the start of simulation ($nt = 0$, nt being the simulation time step) in Fig. 2. The points (circle, square and triangle) are obtained by the PIC code PASUPAT while the curves represent the local field E_l evaluated using the cosine law $E_l(\tilde{\theta}) = E_a \cos \tilde{\theta}$ with E_a computed using PASUPAT. Solid squares, solid triangles and open circles represent surface fields for $E_0 = 1.5$ V/nm, $E_0 = 1.75$ V/nm and $E_0 = 2.0$ V/nm respectively. Initially, there is no particle inside the diode gap and hence there is no space charge effect. It is well established that in the absence of space charge, the electric field at the surface of hemi-ellipsoid follows cosine variation^{22,23}. Fig. 2 shows that fields obtained using PASUPAT agree reasonably well with the cosine law. A similar study for Geometry 1 and 3 also shows that the electric field on the emitter surface follows the cosine law at the start of simulation.

We have calculated the average percentage relative error in the PIC field with respect to local field obtained using the cosine law as follows:

$$\Xi = \frac{1}{N_p} \sum_{\tilde{\theta}_i=0}^{\tilde{\theta}_{R_a}} \frac{|E_a \cos \tilde{\theta}_i - E_{\text{PIC}}(\tilde{\theta}_i)|}{E_a \cos \tilde{\theta}_i} \times 100, \quad (6)$$

where both E_a and E_{PIC} are calculated using PASUPAT. E_a is the field at the apex of the tip ($\tilde{\theta} = 0$) while $E_{\text{PIC}}(\tilde{\theta}_i)$ denotes the field on a point on the surface specified by $\tilde{\theta}_i$. N_p is the number of points between $\rho = 0$

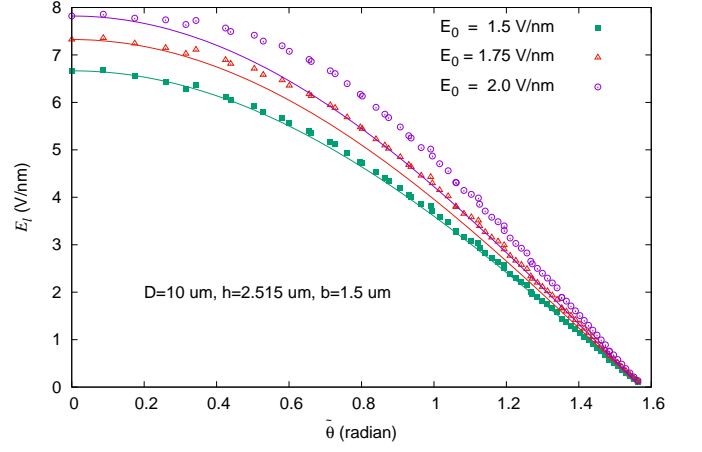


FIG. 3. Variation of electric field on the surface with generalized angle $\tilde{\theta}$ averaged approximately over one transit time using fields obtained every 500 time steps. Three different values of asymptotic electric field E_0 are considered. Points are values obtained using PASUPAT PIC simulation while solid lines correspond to $E_a \cos \tilde{\theta}$. For lower E_0 , the variation of local field follows the cosine law closely, while as E_0 increases, deviation from cosine law is significant.

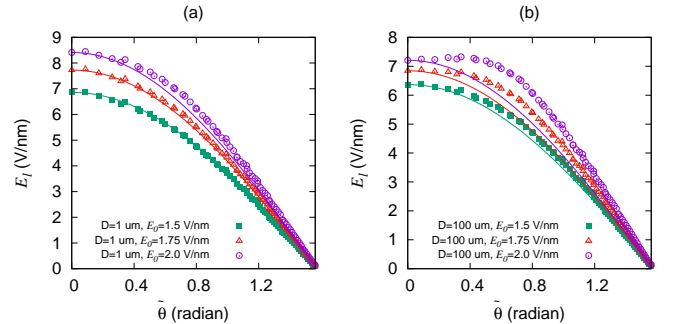


FIG. 4. Variation of time-averaged electric field on the surface with generalized angle $\tilde{\theta}$ for three different values of asymptotic electric field E_0 (a) $D = 1 \mu\text{m}$, $h = 0.2515 \mu\text{m}$ and $b = 0.15 \mu\text{m}$ (Geometry 1) and (b) $D = 100 \mu\text{m}$, $h = 25.15 \mu\text{m}$ and $b = 15 \mu\text{m}$ (Geometry 3). Points are values obtained using PASUPAT PIC simulation and solid lines correspond to $E_a \cos \tilde{\theta}$. For lower E_0 , the field variation follows the cosine law in both cases, while as E_0 increases, deviation from the cosine law is significant for Geometry 3.

to $\rho_m = 3R_a/4$ and $\tilde{\theta}_{R_a}$ corresponds to generalized angle corresponding to ρ_m . For all the cases, $\Xi \approx 1.2\%$ at the start of the simulation⁴¹.

As the simulation proceeds in time, space charge builds up in the diode region and the field at the emitting surface reduces. After about one ballistic transit time, the average emission current settles down to a lower value compared to the start of simulation. We have studied the

variation of the field at the emitter surface, averaged over the fields obtained at intervals of 500 time steps between the second and third transit time. The number of simulation time steps in a single transit time is approximately 3000. Fig. 3 shows the variation of the magnitude of the electric field on the surface of emitter for three asymptotic fields E_0 , 1.5 V/nm, 1.75 V/nm and 2.0 V/nm in case of Geometry 2. As before, points are obtained using the PIC code PASUPAT while the curves represent the cosine law. Solid squares, solid triangles and open circles represent surface fields for $E_0 = 1.5$ V/nm, $E_0 = 1.75$ V/nm and $E_0 = 2.0$ V/nm respectively. It may be seen that the field variation agrees very well with the cosine law for $E_0=1.5$ V/nm while the deviations increase at the largest field.

Apart from the applied field, the validity of the cosine law in the presence of space charge also depends on the size of diode region. This is evident from Fig. 4 which shows the field variation for Geometry 1 (Fig. 4a) and Geometry 3 (Fig. 4b) which differ in size by two orders of magnitude. As before, the variation is averaged using the fields obtained at intervals of 500 time steps between the second and third transit time. As in Fig. 3, solid squares, solid triangles and open circles represent surface fields for $E_0 = 1.5$ V/nm, $E_0 = 1.75$ V/nm and $E_0 = 2.0$ V/nm respectively for both (a) and (b). Solid curves represent the corresponding cosine variation. It may be noted that the local fields are identical in all three cases at the start of the simulation. However Geometry 1 has the smallest transit time and emission area while Geometry 3 has the largest. As a result, Geometry 3 has a larger accumulation of space charge compared to Geometry 1, thus leading to a larger deviation from the cosine law for the same value of applied field. Geometry 1 on the other hand is compatible with the cosine law even at higher values of E_0 .

A measure of space charge is defined as $\vartheta = E_P/E_L$, where E_P is electric field in the presence of space charge and E_L is that obtained by solving Laplace equation³². Here we take E_P as apex electric field averaged from the second to third transit time as before while E_L is the apex field at $nt = 0$. In order to quantify the effect of space charge on the validity of cosine law, the deviation Ξ for different values of ϑ is shown in table II.

It is clear from table II that Ξ is below 3% for $0.9 < \vartheta \leq 1.0$. Thus, in weak space charge limit, cosine law can be used in field emission module of a PIC simulation code.

Another measure of space charge is the scaled current density $\zeta = kJ_P D^2 V^{-3/2}$, where J_P is the space charge affected current density due to field emission of electrons, $V = E_0 D$ is the diode-gap voltage and $k = \epsilon_0^{-1} \sqrt{m/2e}$ is a constant. For planar diode, ϑ and ζ are related to each other as follows^{30,32,42}:

$$3\vartheta^2(1 - \vartheta) = \zeta(4 - 9\zeta). \quad (7)$$

From the above equation, it may be seen that when

TABLE II. Average error for different cases in the presence of space charge

Geometry	E_0 (V/nm)	ϑ	$\Xi(\%)$
1	1.5	0.981	0.57
	1.75	0.947	1.06
	2.0	0.902	2.62
2	1.5	0.953	0.96
	1.75	0.898	3.14
	2.0	0.839	5.88
3	1.5	0.910	2.81
	1.75	0.839	6.32
	2.0	0.773	10.07

$\vartheta \rightarrow 0$, the normalized current $\zeta \rightarrow 4/9$ i.e. $J_P \rightarrow J_{CL}$, where $J_{CL} = (4\epsilon_0/9)(\sqrt{2e/m})(V^{3/2}/D^2)$ is the Child-Langmuir^{43,44} current density.

In the weak space charge regime, $\vartheta \rightarrow 1$ and $\zeta \rightarrow 0$, the solution to above equation around $\zeta = 0$ may be expressed as:

$$\vartheta = 1 - \frac{4}{3}\zeta + \dots \quad (8)$$

Note that in case of planar diode ϑ is ratio of electric field at the cathode in the presence of space charge and $E_0 = V_g/D$.

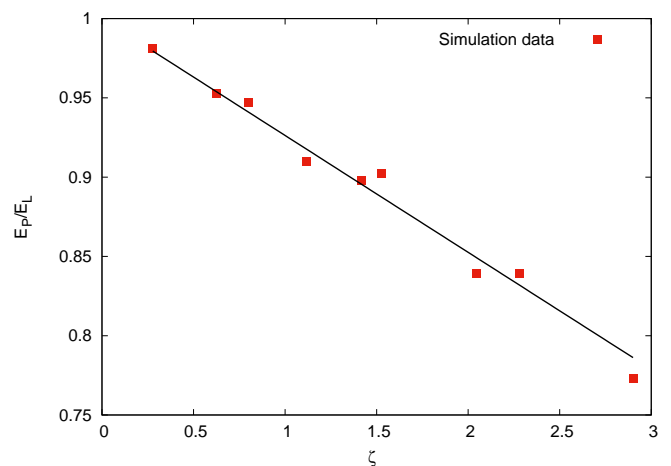


FIG. 5. Normalized apex field $\vartheta = E_P/E_L$ plotted against normalized current ζ for $g = 0.7$. Line $\vartheta = 1.0 - \delta\zeta$ was fitted to the points. Best fit gives $\delta = 0.073$. Best fitted line is also shown with the simulation point.

In case of curved emitters, the relation between ϑ and ζ may involve the field enhancement factor γ_a . This expectation stems from a recent result where it was shown

that for curved emitters, the space charge limited current density scales as $J_{SCL} \simeq \gamma_a J_{CL}^{39}$, here $\gamma_a = E_a/E_0$ is the field enhancement factor at the apex of the tip. Moreover, in case of emission from curved tips, the current density is not uniform over the emission area. Notwithstanding all these complications, we attempt to find a relation like $\vartheta = 1 - \delta\zeta$ by fitting the simulation data, where δ is a constant. However, calculation of ζ requires the current density J_P . To calculate J_P from the current I_P obtained in simulation, we need to divide I_P by emission area \mathcal{A} . First we assume $\mathcal{A} = \pi b^2$, i.e. base of the hemi-ellipsoidal tip. For this case, value of δ is found to be 0.43. But, field emission from curved surfaces is predominantly from the area in the vicinity of the apex of the tip. So a better way to calculate emission area may be to assume area $\mathcal{A} = \pi(gR_a)^2$, where $g \leq 1$. Fig. 5 shows variation of ϑ with ζ obtained using PIC simulation. Here g was taken to be 0.7. A straight line $\vartheta = 1 - \delta\zeta$ is fitted to the simulation points. We obtain $\delta = 0.073$ for the best fit and the points appear to follow this linear trend even for $\vartheta < 0.9$.

TABLE III. Variation of fitting parameter δ with g

g	0.5	0.6	0.7	0.8	0.9	1.0
δ	0.037	0.050	0.073	0.092	0.12	0.152

Table III gives values of δ obtained for different values of g corresponding to different emitting area at the tip. Note that values of δ obtained using simulation for all values of g is quite small compared to $\delta = 4/3$ predicted by Eq. 7 which does not consider correction for the curved emitter. This needs further theoretical investigation with role of field enhancement factor considered properly.

V. CONCLUSIONS

The effect of space charge on the validity of the generalized cosine law of field variation at the surface of hemi-ellipsoidal emitter was investigated using PIC simulations. A special field emission module in PIC code PASUPAT was used for emission of electrons. This module uses the cosine law of field variation to estimate the net current from the emitter. A distribution function based on cosine law is used to calculate the total energy, normal energy and launch angle of computational particles in the present study. It has been found that the average deviation Ξ of the field from cosine law is less than 3% for space charge parameter ϑ lying between 0.9 to 1.0. Thus for cases where space charge is not very strong, the field emission module based on cosine law can be used in PIC codes. As this scheme does not require calculation of current from each cell at the emitting surface, it helps in making the computation faster.

We have also investigated the relation between normalized field at the apex of emitter, ϑ and normalized

diode current ζ for curved emitter. In the weak space charge regime, simulation result shows that ϑ and ζ follow a linear relation similar to that for the flat emitters ($\vartheta = 1 - \delta\zeta$). The value of δ is however small compared to that for the flat emitters. As the space charge limited current for curved emitters depends on the apex field enhancement factor, the theory for space charge affected field emission may need to be modified for curved emitters.

Acknowledgments: R. K. thanks A. K. Poswal, Atomic and Molecular Physics Division, BARC for useful discussions. PASUPAT simulations were performed on ANUPAM-AGANYA super-computing facility at Computer Division, BARC.

Data Availability: The data that supports the findings of this study are available within the article.

- ¹R. H. Fowler and L. Nordheim, Proc. R. Soc. A 119, 173 (1928).
- ²L. W. Nordheim, Proc. R. Soc. A 121, 626 (1928).
- ³R. E. Burgess, H. Kroemer, J. M. Houston, Phys. Rev. 90, 515 (1953).
- ⁴E. L. Murphy and R. H. Good, Phys. Rev. 102, 1464 (1956).
- ⁵K. L. Jensen, J. Vac. Sci. Technol. B 21, 1528 (2003).
- ⁶R. G. Forbes, App. Phys. Lett. 89, 113122 (2006).
- ⁷K. L. Jensen, *Introduction to the physics of electron emission*, Chichester, U.K., Wiley, 2018.
- ⁸R. G. Forbes and J. H. B. Deane, Proc. R. Soc. A 463, 2907 (2007).
- ⁹J. H. B. Deane and R. G. Forbes, J. Phys. A: Math. Theor. 41, 395301 (2008).
- ¹⁰A. Kyritsakis and J. P. Xanthakis, Proc. R. Soc. London A 471, 20140811 (2015).
- ¹¹D. Biswas, Physics of Plasmas 25, 043105 (2018).
- ¹²K. L. Jensen, J. Appl. Phys. 126, 065302 (2019).
- ¹³D. Biswas and R. Ramachandran, J. Vac. Sci. Technol. B 37, 021801 (2019).
- ¹⁴R. Ramachandran and D. Biswas, Journal of Applied Physics, 129, 184301 (2021).
- ¹⁵D. Biswas and R. Ramachandran, Journal of Applied Physics, 129, 194303 (2021).
- ¹⁶R. G. Forbes, Journal of Applied Physics 126, 210901 (2019).
- ¹⁷D. Biswas and R. Kumar, J. Vac. Sci. Technol. B 37, 040603 (2019).
- ¹⁸C. J. Edgcombe, and U. Valdrè, Philosophical Magazine B 82, 987 (2002).
- ¹⁹R. G. Forbes, C. J. Edgcombe, and U. Valdrè, Ultramicroscopy 95, 57 (2003).
- ²⁰D. Biswas, Phys. Plasmas 25, 043113 (2018).
- ²¹S. G. Sarkar and D. Biswas, J. Vac. Sci. Technol. B 37, 062203 (2019).
- ²²D. Biswas, G. Singh, S. G. Sarkar and R. Kumar, Ultramicroscopy 185, 1 (2018)
- ²³D. Biswas, G. Singh and Rajasree R., Physica E, 109, 179 (2019).
- ²⁴C K Birdsall and A. B. Langdon, "Plasma Physics via Computer Simulation", New York: McGraw-Hill, 1985.
- ²⁵S. G. Sarkar, R. Kumar, G. Singh and D. Biswas, Physics of Plasmas 28, 013111 (2021).
- ²⁶The angle θ closely approximates the angle θ_L that the local normal direction makes with respect to the emitter axis¹¹.
- ²⁷D. Biswas, Physics of Plasmas, 26, 073106 (2019).
- ²⁸D. Biswas and R. Rudra, J. Vac. Sci. Technol. B 38, 023207 (2020).
- ²⁹D. Biswas, J. Vac. Sci. Technol. B 38, 023208 (2020).
- ³⁰J. Barbour, W. Dolan, J. Trolan, E. Martin, and W. Dyke, Physical Review 92, 45 (1953).
- ³¹Y. Feng and J. Verboncoeur, Phys. Plasmas 13, 073105 (2006).

- ³²R. Forbes, J. Appl. Phys. 104, 084303 (2008).
³³P. Chen, T. Cheng, J. Tsai, and Y. Shao, Space charge effects in field emission nanodevices, Nanotechnology 20, 405202 (2009).
³⁴K. L. Jensen, D. A. Shiffler, I. M. Rittersdorf, J. L. Lebowitz, J. R. Harris, Y. Y. Lau, J. J. Petillo, W. Tang, and J. W. Luginsland, J. Appl. Phys. 117, 194902 (2015).
³⁵K. Torfason, A. Valfells, and A. Manolescu, Phys. Plasmas 22, 033109 (2015).
³⁶Lawrence N. Dworsky, "Introduction to Numerical Electrostatics Using MATLAB" John Wiley & Sons, Inc. 2014; <https://doi.org/10.1002/9781118758571.ch9>
³⁷J. Loverich, C. Nieter, D. Smithe, S. Mahalingam, and P. Stoltz, 'Charge conserving emission from conformal boundaries in electro-magnetic PIC simulations', available at <https://www.researchgate.net/profile/John-Loverich/publication/>
³⁸J. P. Edelen, N. M. Cook, C. C. Hall, Y. Hu, X. Tan, and J.-L. Vay, J. Vac. Sci. Technol. B 38, 043201 (2020).
³⁹G. Singh, R. Kumar and D. Biswas, Physics of Plasmas 27, 104501 (2020).
⁴⁰W. L. Briggs, V. E. Henson, and S. F. McCormick, 'A Multigrid Tutorial', 2nd Edition, SIAM, ISBN: 978-0-89871-462-3 (2000).
⁴¹Even with a converged solution using the multigrid solver, the process of determining the surface field at the centre of the cut-cell using the cartesian grid induces errors.
⁴²A. Kyritsakis, M. Veske, and F. Djurabekova, New Journal of Physics 23, 063003 (2021).
⁴³C. D. Child, Phys. Rev. 32, 492 (1911).
⁴⁴I. Langmuir, Phys. Rev. 2, 450 (1913).

Appendix: Corrections to the distribution of emitted electrons

In Ref. [11], the distribution of field-emitted electrons on the surface of a locally parabolic sharp emitter was derived using the generalized cosine law. The sharpness assumption resulted in the approximations $R_a/h \rightarrow 0$ and $z/h \rightarrow 1$ where h is the height of emitter, R_a the apex radius of curvature and $z \approx h - \frac{\rho^2}{2R_a}$ is a point on the locally parabolic surface of the axially symmetric emitter. These approximations are good to use when $h/R_a > 50$ but must be replaced by more accurate calculations when the emitter is not so sharp.

The basic equation for the field emission current from a patch $[\rho, \rho + d\rho]$ on the surface of an axially symmetric emitter is

$$dI = f(\rho)d\rho = J_{MG}(\rho)2\pi\rho\sqrt{1 + (dz/d\rho)^2}d\rho \quad (\text{A.1})$$

where $J_{MG}(\rho)$ is the Murphy-Good current density at (ρ, z) where $z \approx h - \frac{\rho^2}{2R_a}$. Since $J_{MG}(\rho)$ depends on the local field $E_l(\rho) = E_a \cos \tilde{\theta}$, where

$$\cos \tilde{\theta} = \frac{\tilde{z}}{\sqrt{\tilde{z}^2 + \tilde{\rho}^2}}, \quad (\text{A.2})$$

it is profitable to study the distribution of electrons with respect to $\tilde{\theta}$ rather than ρ . The scaled variables $\tilde{z} = z/h$ and $\tilde{\rho} = \rho/R_a$ can be used to rewrite Eq. (A.1) as

$$dI = f(\tilde{\theta})d\tilde{\theta} = 2\pi R_a^2 J_{MG}(\tilde{\theta})\tilde{\rho}\sqrt{1 + \tilde{\rho}^2}\frac{d\tilde{\rho}}{d\tilde{\theta}}d\tilde{\theta}. \quad (\text{A.3})$$

In the following, we shall express $f(\tilde{\theta})$ purely in terms of $\tilde{\theta}$ without resorting to the approximations mentioned above.

We shall first express $\sqrt{1 + \tilde{\rho}^2}$ in terms of $\sqrt{\tilde{z}^2 + \tilde{\rho}^2}$ without assuming $\tilde{z} \approx 1$. This can be easily achieved by noting that

$$\begin{aligned} 1 + \tilde{\rho}^2 &= \tilde{z}^2 + \tilde{\rho}^2 + (1 - \tilde{z}^2) = (\tilde{z}^2 + \tilde{\rho}^2)\frac{1 + \tilde{\rho}^2}{\tilde{z}^2 + \tilde{\rho}^2} \\ &= (\tilde{z}^2 + \tilde{\rho}^2)\left(\sin^2 \tilde{\theta} + \frac{\cos^2 \tilde{\theta}}{\tilde{z}^2}\right) \end{aligned} \quad (\text{A.4})$$

Thus, $\sqrt{1 + \tilde{\rho}^2} = C_0\sqrt{\tilde{z}^2 + \tilde{\rho}^2}$ where

$$C_0 = \left(\sin^2 \tilde{\theta} + \frac{\cos^2 \tilde{\theta}}{\tilde{z}^2}\right)^{1/2}. \quad (\text{A.5})$$

The next correction requires an evaluation of $d\tilde{\rho}/d\tilde{\theta}$. To achieve this, first note that for a locally parabolic tip, $\tilde{\rho}^2 \approx (1 - \tilde{z})2h/R_a$. Thus using Eq. (A.2),

$$\tilde{z}^2(\sec^2 \tilde{\theta} - 1) + \frac{2h}{R_a}\tilde{z} - \frac{2h}{R_a} = 0 \quad (\text{A.6})$$

which can be solved to express \tilde{z} in terms of $\tilde{\theta}$ as

$$\tilde{z} = \frac{h}{R_a} \cot^2 \tilde{\theta} \left[\sqrt{1 + \frac{2R_a}{h} \tan^2 \tilde{\theta}} - 1 \right]. \quad (\text{A.7})$$

Finally, using $\sin \tilde{\theta} = \tilde{\rho}/\sqrt{\tilde{\rho}^2 + \tilde{z}^2}$, we have

$$\cos \tilde{\theta} d\tilde{\theta} = \frac{d\tilde{\rho}}{\sqrt{\tilde{\rho}^2 + \tilde{z}^2}} \left[1 - \frac{\tilde{\rho}^2 + \tilde{\rho}\tilde{z}\frac{d\tilde{z}}{d\tilde{\rho}}}{\tilde{\rho}^2 + \tilde{z}^2} \right] \quad (\text{A.8})$$

where $d\tilde{z}/d\tilde{\rho} \approx -\tilde{\rho}R_a/h$ for a locally parabolic tip. On simplification and using Eq. (A.7),

$$\cos \tilde{\theta} d\tilde{\theta} = \frac{\cos^2 \tilde{\theta}}{\sqrt{\tilde{\rho}^2 + \tilde{z}^2}} C_1 d\tilde{\rho} \quad (\text{A.9})$$

where

$$C_1 = \sqrt{1 + \frac{2R_a}{h} \tan^2 \tilde{\theta}}. \quad (\text{A.10})$$

Thus,

$$\frac{d\tilde{\rho}}{d\tilde{\theta}} = \frac{\sqrt{\tilde{\rho}^2 + \tilde{z}^2}}{\cos \tilde{\theta}} \frac{1}{C_1}. \quad (\text{A.11})$$

Putting everything together and using the expressions for $\sin \tilde{\theta}$ and $\cos \tilde{\theta}$, we finally have

$$f(\tilde{\theta}) = 2\pi R_a^2 J_{MG}(\tilde{\theta}) \tilde{\rho} \frac{\tilde{\rho}^2 + \tilde{z}^2}{\cos \tilde{\theta}} \frac{C_0}{C_1} \quad (\text{A.12})$$

$$= 2\pi R_a^2 J_{MG}(\tilde{\theta}) \frac{\sin \tilde{\theta}}{\cos^4 \tilde{\theta}} \times \tilde{z}^3 \frac{C_0}{C_1} \quad (\text{A.13})$$

where the correction factor $\tilde{z}^3 C_0/C_1$ can be evaluated using Eqns. (A.5), (A.7), and (A.10).